Contributions to Geophysics and Geodesy Vol. 55/2, 2025 (201–221)

An enhancement filter utilizing the modified arctangent function for the structural and tectonic interpretation of causative sources: Application to WGM2012 gravity data from the Rafsanjan Plain, Iran

Fengjun WU*, Xin-Ai XU

School of Mathematics and Information Science, Nanchang Normal University, Nanchang, 330032, China;
e-mails: wfj@ncnu.edu.cn; jxxxa@ncnu.edu.cn

Abstract: Gravity data edge detection methods play a crucial role in identifying the horizontal positions of buried sources and enhancing the interpretation of subsurface structures. Among these methods, the Total Horizontal Gradient (THG) filter is widely used due to its noise stability and straightforward formulation. However, the THG filter has inherent limitations, prompting the development of refined edge detection techniques. To address these shortcomings, various approaches based on local phase analysis or normalized filters have been introduced, many of which incorporate the arctangent function to combine horizontal and vertical gradients. While these methods improve edge detection, they also exhibit drawbacks, such as the generation of spurious edges and restricted resolution. In this study, we propose the Modified Arctangent Function (MAT), which enhances gravity source edge detection by integrating the total horizontal gradient with a modified arctangent function. The effectiveness of the MAT filter is systematically evaluated against conventional filters that utilize the arctangent function and/or the total horizontal gradient. Its performance is validated through synthetic gravity data tests, both with and without noise contamination. To further assess its applicability, the MAT filter is applied to high-resolution gravity data from the WGM2012 (World Gravity Map) over the Rafsanjan Plain in Iran. Additionally, an approximated derivative calculation method is incorporated to mitigate noise amplification during the derivative computation process. The results from both synthetic and real data confirm that the MAT filter effectively detects and delineates gravity anomalies, demonstrating its potential as a valuable tool for geophysical interpretation.

Key words: edge detection, WGM2012, gravity anomaly, Rafsanjan plain (Iran)

*corresponding author, e-mail: wfj@ncnu.edu.cn

doi: 10.31577/congeo.2025.55.2.5

1. Introduction

Gravity method is valuable for solving a wide range of geological problems, including mineral exploration, fault mapping, and subsurface geological modelling (*Ekinci et al., 2023; Elhussein and Diab, 2023, 2025; Ai et al., 2024a*). Detecting the edges of causative sources is a crucial task in gravity data interpretation (*Saada et al., 2021, 2025; Hamimi et al., 2023; Alvandi et al., 2023; Farhi et al., 2025*). Gravity anomalies reflect the combined effects of sources at various depths and positions, as well as sources with differing density contrasts. As a result, the observed anomaly often contains a mix of both weak and strong signal intensities within the same dataset. Most existing edge detection methods are based on the vertical and horizontal gradients of gravity data, but these techniques often suffer from limitations, such as generating spurious edges, low resolution, and unbalanced amplitude output (*Ekwok et al., 2022a,b; Alvandi and Ardestani, 2023; Ai et al., 2024b, 2024c; Deniz Toktay et al., 2024; Alvandi et al., 2023, 2024, 2025; Eldosouky et al., 2022, 2024a,b; Pham et al., 2022; Pham and Prasad, 2023; Ghiasi et al., 2023; Hosseini et al., 2024; Akpa et al., 2024*).

One widely used approach is the Total Horizontal Gradient (THG) filter, introduced by *Cordell and Grauch (1985)*, which is a fundamental tool in geophysical data interpretation. The THG is defined as:

$$\mathrm{THG} = \sqrt{\left(\frac{\partial \mathrm{G}}{\partial x}\right)^2 + \left(\frac{\partial \mathrm{G}}{\partial y}\right)^2}. \tag{1}$$

To overcome the limitations of the THG filter, local phase filters were introduced to balance weak and strong signals from bodies at varying depths. These filters often leverage directional derivatives and the arctangent function to enhance edge detection. *Miller and Singh (1994)* proposed the Tilt Angle (TA) method, which combines the vertical gradient with the total horizontal gradient of the gravity field:

$$\mathrm{TA} = \tan^{-1}\left[\frac{\frac{\partial \mathrm{G}}{\partial z}}{\mathrm{THG}}\right]. \tag{2}$$

Cooper and Cowan (2006) introduced the Horizontal Tilt Angle (TDX) method, which also uses the THG but inverts the ratio to delineate edges more distinctly than the TA method:

$$\mathrm{TDX} = \tan^{-1}\left[\frac{\mathrm{THG}}{\left|\frac{\partial \mathrm{G}}{\partial z}\right|}\right]. \tag{3}$$

Despite their effectiveness, both the TA and TDX methods can generate false edges in noisy data (*Alvandi and Ardestani, 2023*). To refine these methods, *Ferreira et al. (2013)* proposed the Tilt Angle of the total Horizontal Gradient (TAHG), which incorporates the directional derivatives of the THG:

$$\mathrm{TAHG} = \tan^{-1}\left[\frac{\frac{\partial \mathrm{THG}}{\partial z}}{\sqrt{\left(\frac{\partial \mathrm{THG}}{\partial x}\right)^2 + \left(\frac{\partial \mathrm{THG}}{\partial y}\right)^2}}\right]. \tag{4}$$

The TAHG technique utilizes the directional derivatives of the total horizontal gradient in conjunction with the arctangent function.

Ma et al. (2016) introduced the Improved Normalized Horizontal Gradient (ITDX) method, which employs the second vertical derivative of the gravity field to enhance edge detection and suppress noise:

$$\mathrm{ITDX} = \tan^{-1}\left[\frac{\sqrt{\left(\frac{\partial^2 \mathrm{G}}{\partial z \partial x}\right)^2 + \left(\frac{\partial^2 \mathrm{G}}{\partial z \partial y}\right)^2}}{\left|\frac{\partial^2 \mathrm{G}}{\partial z^2}\right|}\right]. \tag{5}$$

The second vertical derivative in Eq. (5) is calculated using Laplace's equation to reduce noise effects:

$$\frac{\partial^2 \mathrm{G}}{\partial z^2} = -\frac{\partial^2 \mathrm{G}}{\partial x^2} - \frac{\partial^2 \mathrm{G}}{\partial y^2}. \tag{6}$$

Nasuti et al. (2019) proposed the Total Horizontal Gradient of the Second-Order Tilt Derivative (THSTD) filter:

$$\mathrm{THSTD} = \sqrt{\left(\frac{\partial \mathrm{STD}}{\partial x}\right)^2 + \left(\frac{\partial \mathrm{STD}}{\partial y}\right)^2}, \tag{7}$$

where

$$\mathrm{STD} = \tan^{-1}\left[\frac{\mathrm{R}\times\dfrac{\partial^2\mathrm{G}}{\partial z^2}}{\sqrt{\left(\dfrac{\partial\mathrm{THG}}{\partial x}\right)^2+\left(\dfrac{\partial\mathrm{THG}}{\partial y}\right)^2}}\right]. \tag{8}$$

In Equation (8), R represents the average value of the gravity field, and the second derivative of G with respect to z, denoted as $\partial^2\mathrm{G}/\partial z^2$, is also derived from Laplace's equation. These evolving techniques highlight the continuous effort to enhance edge detection accuracy, balancing the resolution of subtle features with robustness against noise.

2. Proposed technique

We here introduce a resolution filter that employs the Modified Arctangent Function. This filter is based on the arctangent function, which plays a crucial role in the design of edge detection filters, such as TA, TDX, TAHG, ITDX, and THSTD. The proposed filter (MAT) is inspired by the tilt angle of the total horizontal gradient filter developed by *Ferreira et al. (2013)* and a recent work of *Alvandi et al. (2025)* and is formulated as a modified arctangent filter. The equation for the MAT technique is presented as follows:

$$\mathrm{MAT} = \frac{2}{\pi}\tan^{-1}(2\mathrm{E}-1)\,, \tag{9}$$

where:

$$\mathrm{E} = \frac{\left(2\dfrac{\partial\mathrm{THG}}{\partial z}\right)-\left(\sqrt{\left(\dfrac{\partial\mathrm{THG}}{\partial x}\right)^2+\left(\dfrac{\partial\mathrm{THG}}{\partial y}\right)^2}\right)}{\sqrt{\left(\dfrac{\partial\mathrm{THG}}{\partial x}\right)^2+\left(\dfrac{\partial\mathrm{THG}}{\partial y}\right)^2+\left(\dfrac{\partial\mathrm{THG}}{\partial z}\right)^2}}\,. \tag{10}$$

The amplitude peak of the introduced filter is situated at the edges of the gravity anomaly. The filter's amplitude ranges from -1 to $+1$ radians. Unlike some edge detection filters, such as the THSTD filter, the MAT filter does not require the specification of a parameter to enhance resolution. Notably, the construction of MAT is similar to the Modified Gudermannian Function (MGTHG) method presented within *Alvandi et al. (2025)* with the difference of the normalized term within the arctangent function. Therefore, the two methods are capable of achieving similar performance for indicating edges. The noise attenuation method within this study is different from *Alvandi et al. (2025)*.

3. Mitigating the effect of noise

The partial derivatives $\partial\mathrm{G}/\partial\mathrm{x}$ and $\partial\mathrm{G}/\partial\mathrm{y}$ are calculated using the finite difference method. This study employs the effective approach introduced by *Tran and Nguyen (2020)* to compute $\partial\mathrm{G}/\partial\mathrm{z}$ and $\partial^2\mathrm{G}/\partial\mathrm{z}^2$, thereby mitigating the effects of noise, as noted by *Oliveira and Pham (2022)*. In the Cartesian coordinate system, let us consider the function as representing a potential field measured at a height, with the positive z-axis oriented vertically downward. The upward continuation fields $\mathrm{G}(x, y, z-\Delta\mathrm{L})$, $\mathrm{G}(x, y, z-2\Delta\mathrm{L})$, $\mathrm{G}(x, y, z-m\Delta\mathrm{L})$, at the heights $\Delta\mathrm{L}, 2\Delta\mathrm{L}, ..., m\Delta\mathrm{L}$, with $n = m = 1, 2, 3...N$, are described by *Tran and Nguyen (2020)*:

$$\begin{cases} \mathrm{G}(-\Delta\mathrm{L}) = \mathrm{G} - \Delta\mathrm{L}\dfrac{\partial\mathrm{G}}{\partial z} + \dfrac{(-\Delta\mathrm{L})^2}{2!}\dfrac{\partial^2\mathrm{G}}{\partial z^2} + \cdots + \dfrac{(-\Delta\mathrm{L})^n}{n!}\dfrac{\partial^n\mathrm{G}}{\partial z^n} \\ \mathrm{G}(-\Delta 2\mathrm{L}) = \mathrm{G} - 2\Delta\mathrm{L}\dfrac{\partial\mathrm{G}}{\partial z} + \dfrac{(-2\Delta\mathrm{L})^2}{2!}\dfrac{\partial^2\mathrm{G}}{\partial z^2} + \cdots + \dfrac{(-2\Delta\mathrm{L})^n}{n!}\dfrac{\partial^n\mathrm{G}}{\partial z^n} \\ \mathrm{G}(-m\Delta\mathrm{L}) = \mathrm{G} - m\Delta\mathrm{L}\dfrac{\partial\mathrm{G}}{\partial z} + \dfrac{(-m\Delta\mathrm{L})^2}{2!}\dfrac{\partial^2\mathrm{G}}{\partial z^2} + \cdots + \dfrac{(-m\Delta\mathrm{L})^n}{n!}\dfrac{\partial^n\mathrm{G}}{\partial z^n} \end{cases} \tag{11}$$

with $n = 3$, Eq. (11) becomes:

$$\begin{cases} \mathrm{G}(-\Delta\mathrm{L}) = \mathrm{G} - \Delta\mathrm{L}\dfrac{\partial\mathrm{G}}{\partial z} + \dfrac{(-\Delta\mathrm{L})^2}{2!}\dfrac{\partial^2\mathrm{G}}{\partial z^2} + \cdots + \dfrac{(-\Delta\mathrm{L})^3}{3!}\dfrac{\partial^3\mathrm{G}}{\partial z^3} \\ \mathrm{G}(-\Delta 2\mathrm{L}) = \mathrm{G} - 2\Delta\mathrm{L}\dfrac{\partial\mathrm{G}}{\partial z} + \dfrac{(-2\Delta\mathrm{L})^2}{2!}\dfrac{\partial^2\mathrm{G}}{\partial z^2} + \cdots + \dfrac{(-2\Delta\mathrm{L})^3}{3!}\dfrac{\partial^3\mathrm{G}}{\partial z^3} \\ \mathrm{G}(-3\Delta\mathrm{L}) = \mathrm{G} - 3\Delta\mathrm{L}\dfrac{\partial\mathrm{G}}{\partial z} + \dfrac{(3\Delta\mathrm{L})^2}{2!}\dfrac{\partial^2\mathrm{G}}{\partial z^2} + \cdots + \dfrac{(-3\Delta\mathrm{L})^3}{3!}\dfrac{\partial^3\mathrm{G}}{\partial z^3} \end{cases} \tag{12}$$

Solving the equations above, the vertical gradients $\partial\mathrm{G}/\partial\mathrm{z}$ and $\partial^2\mathrm{G}/\partial\mathrm{z}^2$ can be expressed as follows:

$$\begin{cases} \dfrac{\partial\mathrm{G}}{\partial z} = \dfrac{11\mathrm{G}(x,y,z) - 18\mathrm{G}(x,y,z-\Delta\mathrm{L}) + 9\mathrm{G}(x,y,z-2\Delta\mathrm{L}) - 2\mathrm{G}(x,y,z-3\Delta\mathrm{L})}{6\Delta\mathrm{L}} \\ \dfrac{\partial^2\mathrm{G}}{\partial z^2} = \dfrac{2\mathrm{G}(x,y,z) - 5\mathrm{G}(x,y,z-\Delta\mathrm{L}) + 4\mathrm{G}(x,y,z-2\Delta\mathrm{L}) - \mathrm{G}(x,y,z-3s\Delta\mathrm{L})}{6\Delta\mathrm{L}^2} \end{cases} \tag{13}$$

Similarly as in *Tran and Nguyen (2020)*, the value of ΔL is typically selected to be between 0.1 and 2 times the grid spacing, depending on the quality of the gravity data. In instances where the data exhibits significant levels of noise, the value of ΔL surpasses twice the grid spacing. In this study, through trial-and-error, ΔL is defined as equal to the grid spacing for noise-free data; however, for noisy data, it is set to three times greater than the grid spacing.

In the following sections, the effectiveness of the proposed technique, MAT, will be evaluated by comparing its results with those obtained from other detectors, including THG, TA, TDX, TAHG, ITDX, and THSTD.

4. Synthetic examples

In order to assess the effectiveness of edge detection filters, both a two-dimensional synthetic gravity model and a three-dimensional synthetic model have been developed.

4.1. 2D model

To enhance the clarity of the proposed method's efficacy, a two-dimensional model was developed using sources with both positive and negative density contrasts, as illustrated in Fig. 1. The gravity anomaly is depicted in Fig. 1a, while Figs. 1b through 1h present various representations, including THG, TA, TDX, TAHG, ITDX, THSTD, and MAT. Notably, MAT exhibits a higher resolution in mapping all edges compared to the other methods, and the proposed technique effectively avoids delineating false boundaries between and around the causative sources.

4.2. 3D model

The effectiveness of the presented technique is evaluated using synthetic gravity data, both with and without noise. The first scenario examines a model featuring three causative sources, which are illustrated in perspective and plan views in Fig. 2. Table 1 lists the characteristics of the buried sources. Strikes of the three bodies are 45 degrees. The algorithm developed by *Rao et al. (1990)* was employed to calculate the gravity anomalies of these bodies at observation points measuring 121 km by 121 km, with a sampling

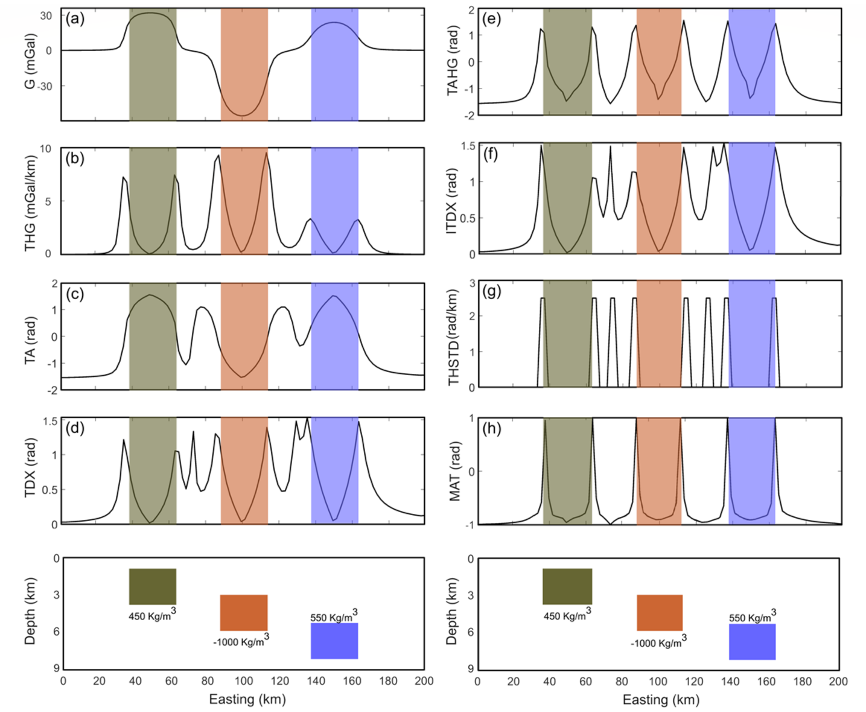

Fig. 1. Two-dimensional gravity model with positive and density contrasts: a) Gravity anomaly, b) THG, c) TA, d) TDX, e) TAHG, f) ITDX, g) THSTD, and h) MAT.

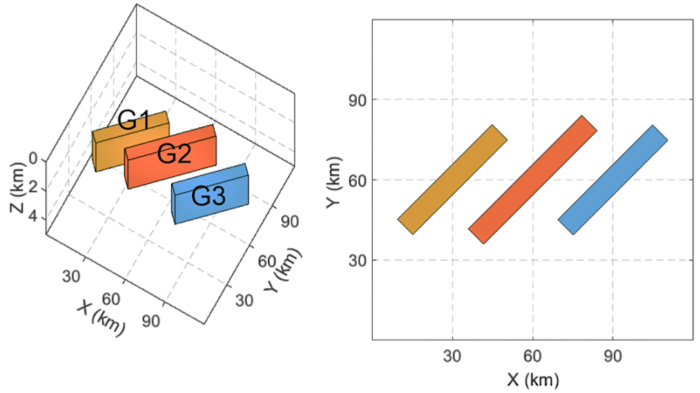

Fig. 2. A three-dimensional representation (a) of the gravity model; a plan view (b).

interval of 1 km.

Table 1. Geometric parameters and designations of the synthetic gravity sources.

Parameters/Label	**G1**	**G2**	**G3**
The center x coordinate (km)	30	60	90
The center y coordinate (km)	60	60	60
The source width (km)	8	8	8
The source length (km)	50	60	50
Depth to the top of the source (km)	2	1	1.8
Density contrast (kg/m^3)	100	−200	300

The gravitational anomaly of the synthetic model is illustrated in Fig. 3a. The results of applying various edge detection methods to this anomaly are shown in Figs. 3b–3h. The THG method (Fig. 3b) highlights the large amplitude responses from the shallow sources G3 and G2, but the boundaries of the deeper source G1 are poorly resolved, with low-definition edges. The TA map (Fig. 3c) struggles to delineate horizontal boundaries, introducing spurious edge information around source G2. The TDX filter (Fig. 3d) successfully maps all source boundaries but produces diffuse edges and false boundary artefacts around structures. Similarly, the TAHG filter (Fig. 3e) captures edges at varying depths but yields low-resolution results. The ITDX filter (Fig. 3f) weakly represents source edges and generates false boundaries around source G2, while the THSTD filter (Fig. 3g) reveals sharp anomaly boundaries but similarly introduces false contours. In contrast, the MAT filter (Fig. 3h) accurately delineates all source boundaries with high resolution, effectively capturing both shallow and deep structures without generating artificial edges.

In the second scenario, the data is contaminated with 3% Gaussian noise. To assess the sensitivity of edge detection methods based on directional derivatives, noise reduction techniques are deliberately omitted to examine the direct impact of noise. The results of edge detection using noisy data are illustrated in Fig. 4. The THG method exhibits lower sensitivity to noise, as it relies solely on the horizontal derivative in its equation. However, this approach fails to detect the edges of deeper sources. In contrast, the TA and TDX methods show higher sensitivity due to their inclusion of the vertical derivative, which enhances source localization but intro-

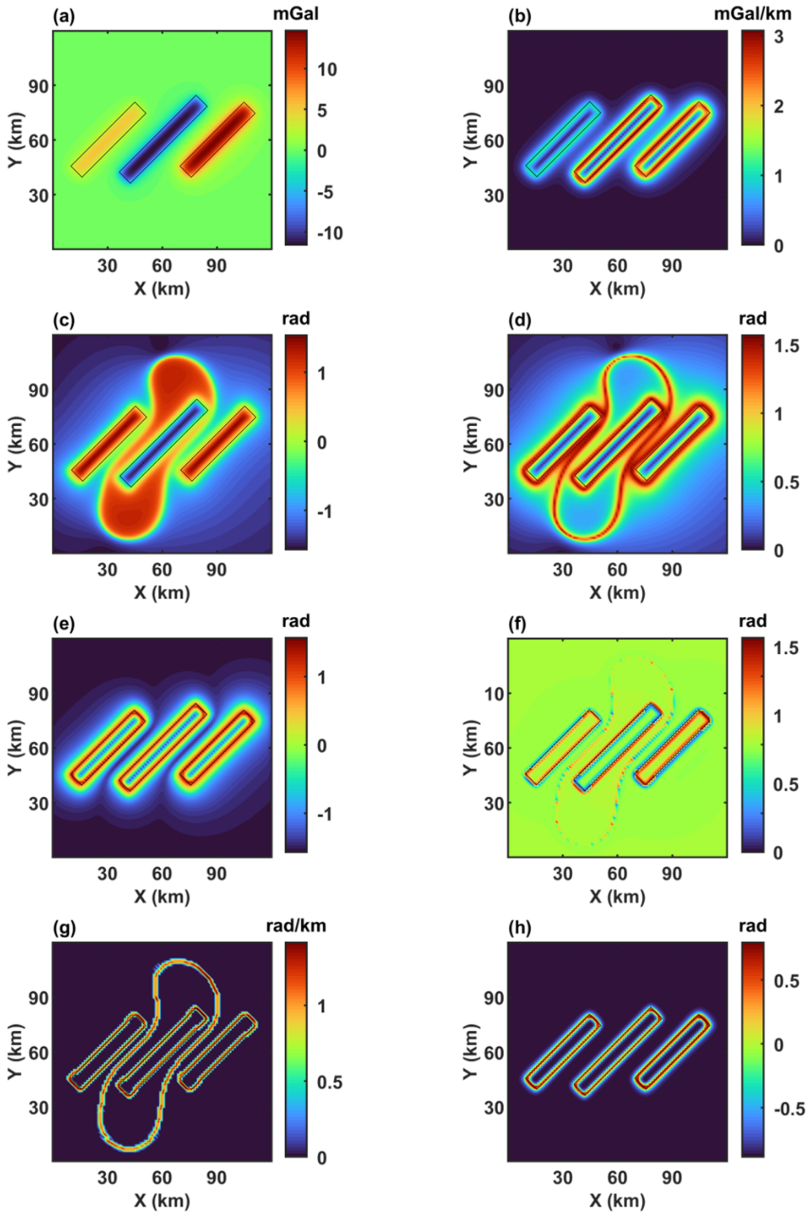

Fig. 3. a) Gravity anomaly of the synthetic model, b) THG, c) TA, d) TDX, e) TAHG, f) ITDX, g) THSTD, and h) MAT (black lines indicate the actual edges).

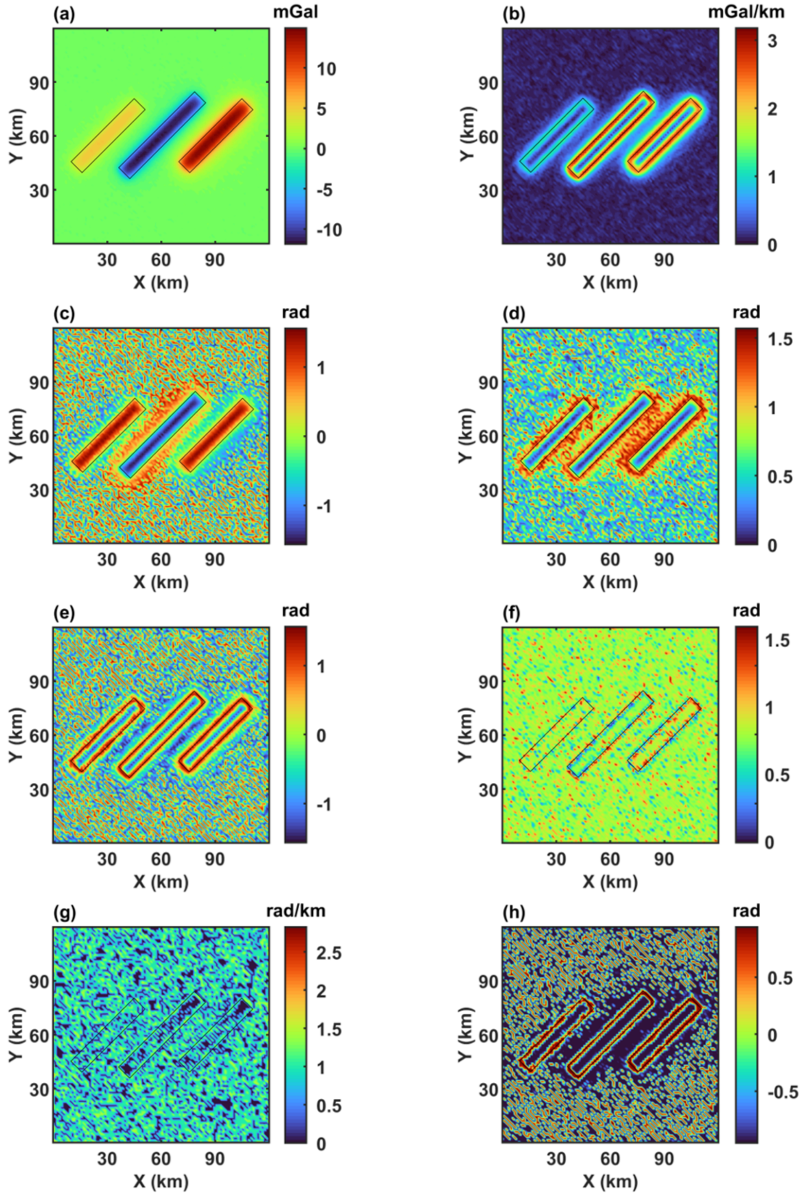

Fig. 4. a) Noisy gravity anomaly of the synthetic model, b) THG, c) TA, d) TDX, e) TAHG, f) ITDX, g) THSTD, and h) MAT (black lines indicate the actual edges).

duces numerous spurious edges that complicate interpretation. Notably, the boundary of the negative density source appears excessively large and displaced from its actual position. The TAHG method, despite the absence of spurious edges, remains highly sensitive to noise because its equation incorporates directional derivatives of the total horizontal gradient. Consequently, noise suppression techniques are crucial before applying this filter to field data. Similarly, the ITDX and THSTD methods, which involve second-order derivatives, are highly susceptible to noise, making it difficult to distinguish true source boundaries, even when preliminary information about their locations is available. As a result, these methods not only produce false edges in noise-free conditions but also perform poorly in noisy environments. Although the proposed MAT filter successfully delineates the three-source edges, it also exhibits noise sensitivity. Therefore, to achieve optimal results, noise reduction techniques should be applied prior to edge detection.

In the third scenario, the method introduced by Tran and Nguyen (2020) is employed to mitigate the effects of noise. The first and second-order orthogonal derivatives have been calculated using this technique. The results of edge detection on noisy data demonstrate the effectiveness of the proposed MAT technique in identifying edges (Fig. 5). In fact, similar to the scenario with noise-free data, if we have high-quality data that is free of noise, we can generate a high-quality map.

5. Real world example

The enhancement and delineation of the edges of anomalous sources play a fundamental role in interpreting potential field data. When discussing the edges of buried sources, this typically refers to fault lines and geological boundaries or rock units that exhibit varying magnetic properties or density contrasts. Consequently, selecting a practical field case that accounts for these conditions is particularly important. For this purpose, the Rafsanjan Plain region has been chosen for analysis due to the presence of various faults at different depths, which allows for the evaluation of edge-determination filters. In this study, the positions and locations of potential geological structures are identified using both conventional edge-determination filters and the proposed filter.

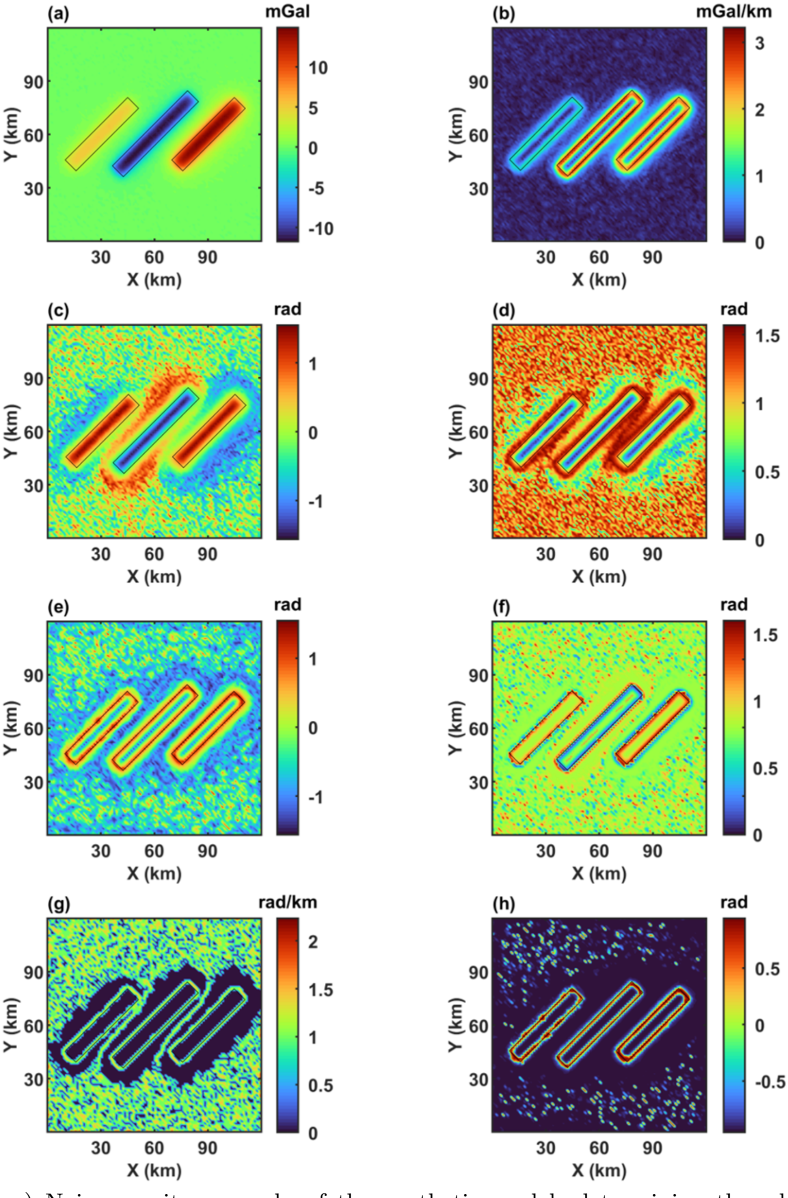

Fig. 5. a) Noisy gravity anomaly of the synthetic model; determining the edge after applying the noise reduction method using the following techniques: b) THG, c) TA, d) TDX, e) TAHG, f) ITDX, g) THSTD, and h) MAT (black lines indicate the actual edges).

5.1. Geology of Rafsanjan Plain

The study area of the Rafsanjan Plain is located in the Posht Badam block. A notable characteristic of this block is the presence of metamorphic outcrops dating back to the Precambrian era, which primarily consist of volcanic, volcanic-clastic, and pyroclastic rocks, as well as calcareous and dolomitic marbles. The magmatic rocks in this block extend beyond the Precambrian; the Late Precambrian to Early Cambrian sequences are associated with alkaline lavas of rift origin. It appears that the phenomenon of rifting, characterized by the opening and formation of an ocean, is a defining feature of this block. In this region, Upper Paleozoic to Jurassic rocks are distributed in a limited manner and have undergone metamorphism. It seems that the recurrence of metamorphic processes during the Late Precambrian, Late Triassic, and Middle Jurassic periods may still characterize these rocks (*Hosseininia and Hassanzadeh, 2023*). The study area has been selected from the previously mentioned block. This region contains deep, well-documented faults that can serve as a valuable resource for evaluating the effectiveness of edge detection filters. The study area is located between 55° and 56° East longitude and 30° and 31° North latitude. Four prominent faults—Rafsanjan (RF), Anar (AF), Shahrbabak (SF), and Davaran (DF)—are found within this region (*Fattahi et al., 2011*). The geological map of the study area is illustrated in Fig. 6.

To evaluate the performance of edge detection filters on real data, gravity data were extracted and analysed from the WGM2012 global model (*Bonvalot et al., 2012*). This model is a widely recognized reference, providing high-quality, freely accessible Earth gravity data through the website (`https://bgi.obs-mip.fr/`). The Bouguer gravity anomaly map of the study area, measured in milligals, is shown in Fig. 7a. Consistent with the approach used for synthetic data, edge detection filters were applied to enhance the interpretability of the field anomaly map. The approximated derivative calculation method introduced by *Tran and Nguyen (2020)* is also employed to suppress the amplified short-wavelength anomalies during the derivative calculation process, resulting in a more coherent edge detection map for analysis.

The results of applying various edge detection methods — including THG, TA, TDX, TAHG, ITDX, THSTD, and the proposed MAT filter — are presented in Figs. 7b–7h. The THG method proves ineffective in

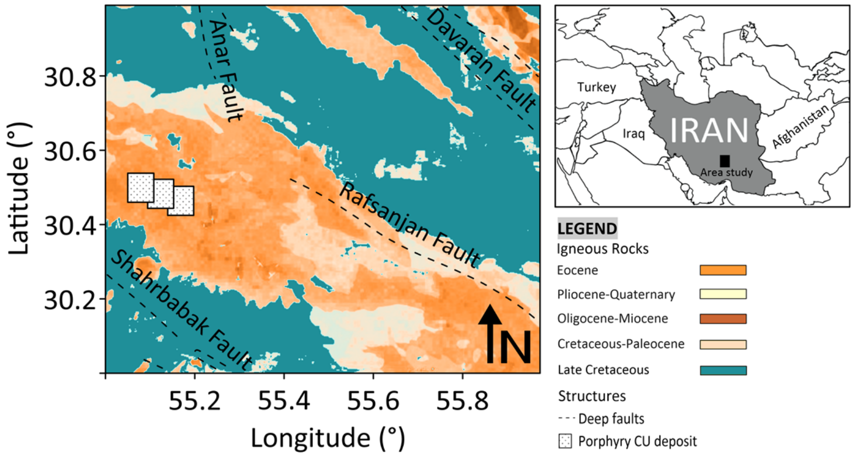

Fig. 6. Geological map of the study area, showing coverage of the most important structural and tectonic features (*Richards and Sholeh, 2016*).

accurately identifying the locations of deep faults. The TA map fails to delineate sharp or distinct boundaries, while the TDX map successfully highlights fault locations but suffers from the drawback of interconnected, indistinct edges. The TAHG map outlines the fault edges, but with insufficient resolution. Similarly, the ITDX and THSTD methods identify fault locations, yet the presence of spurious contours complicates accurate interpretation. In contrast, the results obtained using the proposed MAT filter (Fig. 7) demonstrate its effectiveness in accurately delineating primary faults and other subsurface structures with satisfactory resolution. The filter integrated with the approximated derivative calculation method is capable of balancing edge sharpness and noise suppression, making it a powerful tool for interpreting complex gravity anomaly maps.

6. Discussion

As previously mentioned, the derivative calculation process amplifies short-wavelength noise, which can degrade edge-detection maps and hinder the extraction of useful structural information. To mitigate this issue, various methods have been introduced. These include finite difference-based techniques for vertical derivative computation, such as the backward finite difference method (*Florio et al., 2006*), the fourth-order Tran-Nguyen formula

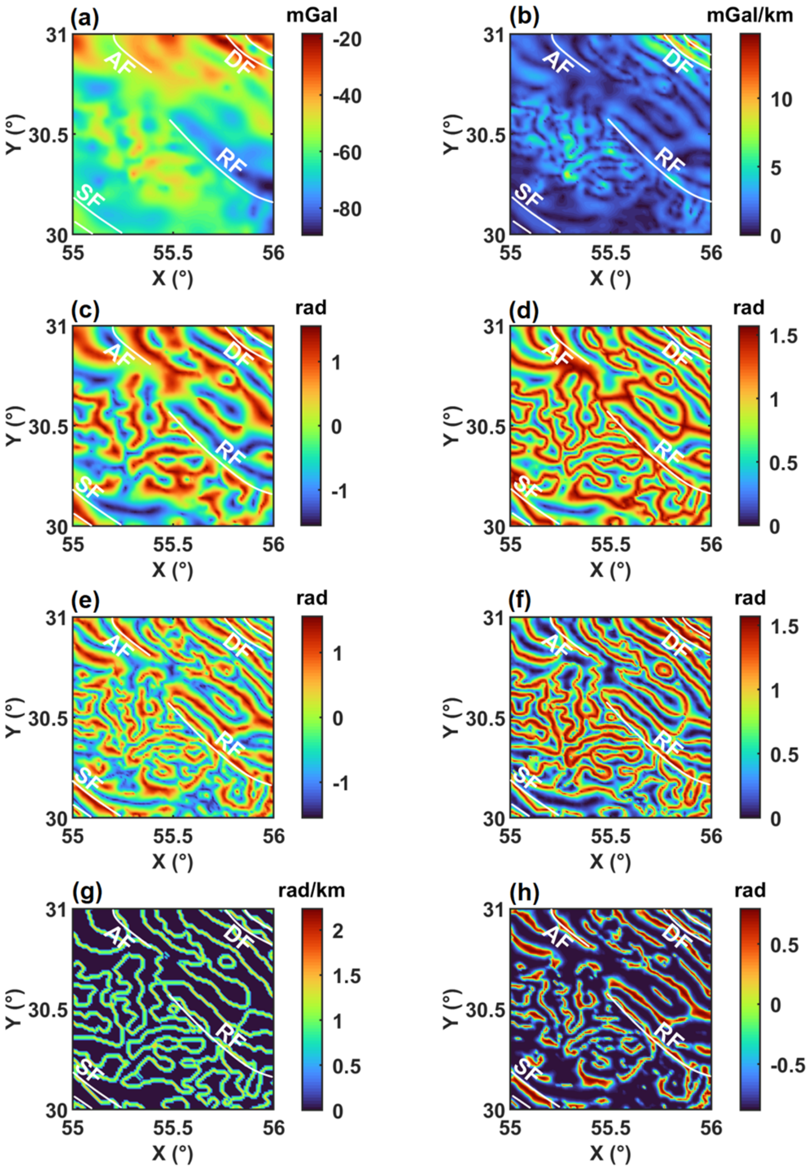

Fig. 7. a) Gravity anomaly of the real model extracted from WGM2012; b) THG; c) TA; d) TDX; e) TAHG; f) ITDX; g) THSTD; and h) MAT (white lines indicate the major faults: Sharbabak (SF), Anar (AF), Rafsanjan (RF), and Davaran (DF)).

(*Tran and Nguyen, 2020*), and the β-vertical derivative (β-VDR) technique (*Oliveira and Pham, 2022*). Additionally, noise suppression techniques applied before gradient calculation, such as the Non-Local Means (NLM) filter and the Modified Non-Local Means (MNLM) filter (*Ai et al., 2023*), have been proposed. In this study, we adopted the method proposed by *Tran and Nguyen (2020)* to address noise amplification. However, the selection of optimal or quasi-optimal parameters still relies on a classical trial-and-error approach. Future research will focus on developing automated or more objective strategies for determining these controlling parameters.

Moreover, the results obtained from the newly proposed edge enhancement method can be used to effectively constrain the horizontal distribution of solutions derived from tilt depth (TD) and Euler deconvolution (ED), providing an estimate of the vertical position of buried structures. ED was initially introduced by *Thompson (1982)* and later generalized to gridded magnetic data by *Reid et al. (1990)*. Early ED algorithms employ a moving window that scans the dataset to estimate depths but often produce a high number of spurious solutions. The successful application of ED depends on effectively distinguishing meaningful results from unphysical solutions, as well as selecting appropriate structural indices and window sizes. The TD method (*Salem et al., 2007; Oruç, 2011*) is also well established for estimating the top depths of target structures without requiring prior knowledge of the source's structural index. However, TD can yield inaccurate depth estimates due to noise in the field data, strong geophysical property contrasts, or the complex shapes of buried structures. To improve the reliability of depth estimation and achieve the horizontal and vertical estimations simultaneously, future work will focus on integrating the newly proposed edge detector with TD and ED methods (*Castro et al., 2020*).

7. Conclusion

Identifying the edges of gravity anomalies is a critical component of geophysical data interpretation, as it helps define the boundaries of subsurface structures and improves overall geological understanding. In this study, we introduced the Modified Arctangent Function (MAT) filter, which integrates the total horizontal gradient with a modified arctangent function to enhance gravity source edge detection. The MAT filter was systematically evaluated against existing edge detection methods that rely on the arctangent function and/or the total horizontal gradient. Its performance was assessed using both noise-free and noise-contaminated synthetic gravity data to ensure its robustness under different data conditions. To mitigate the issue of noise amplification, which commonly affects derivative-based edge detection methods, we incorporated an approximated derivative calculation technique. This procedure helps stabilize the results and improves the clarity of detected boundaries, making the method more effective for real-world applications. The filter was then applied to high-resolution gravity data from the WGM2012 (World Gravity Map) over the Rafsanjan Plain in Iran, an area known for its complex subsurface structures. The results demonstrate that the MAT filter successfully delineates gravity anomaly edges with improved accuracy and resolution compared to conventional methods.

Overall, the MAT filter combined with an approximated derivative calculation technique provides a reliable and effective tool for gravity data interpretation, offering enhanced boundary detection while maintaining robustness against noise. Its ability to accurately highlight subsurface structures makes it highly applicable to a wide range of geophysical studies, including mineral exploration, fault mapping, and subsurface geological modelling. Future research could further refine the method by integrating more advanced noise suppression techniques and combining it with representative depth estimation methods for generating more reliable horizontal and vertical estimations.

Author contributions. All authors have contributed to the conceptualization of this research and computer implementation of the methods. All authors have read and agreed to the published version of the manuscript.

Conflict of interest. The authors state no conflicts of interest relevant to this study.

Acknowledgements. We are very grateful to Dr. Peter Vajda and two anonymous reviewers for their constructive comments and suggestions that have improved the quality of the paper.

Funding. The author(s) declare that financial support was received for the research, authorship, and/or publication of this article. This study was funded by the University Humanities and Social Sciences Research Project of Jiangxi Province (grant number: JC20121).

References

Ai H., Alvandi A., Ghanati R., Pham L. T., Alarifi S. S., Nasui D., Eldosouky A. M., 2023: Modified non-local means: A novel denoising approach to process gravity field data. Open Geosci., **15**, 1, 20220551, doi: 10.1515/geo-2022-0551.

Ai H., Essa K. S., Ekinci Y. L., Balkaya Ç., Géraud Y., 2024a: Hunger Games Search optimization for the inversion of gravity anomalies of active mud diapir from SW Taiwan using inclined anticlinal source approximation. J. Appl. Geophys., **227**, 105443, doi: 10.1016/j.jappgeo.2024.105443.

Ai H., Deniz Toktay H., Alvandi A., Pašteka R., Su K., Liu Q., 2024b: Advancing potential field data analysis: the Modified Horizontal Gradient Amplitude method (MHGA). Contrib. Geophys. Geod., **54**, 2, 119–143, doi: 10.31577/congeo.2024.54.2.1.

Ai H., Ekinci Y. L., Alvandi A., Deniz Toktay H., Balkaya Ç., Roy A., 2024c: Detecting edges of geologic sources from gravity or magnetic anomalies through a novel algorithm based on hyperbolic tangent function. Turk. J. Earth Sci., **33**, 6, 684–701, doi: 10.55730/1300-0985.1936.

Akpa C., Ani C. C., Ekwok S. E., Alzahrani H., Abdelrahman K., Andráš P., Adelekan A., Eldosouky A. M., 2024: Insights into Afikpo Synclinorium structures: Subsurface analysis and intrusion outlining from airborne magnetic data. J. Afr. Earth Sci., **218**, 105374, doi: 10.1016/j.jafrearsci.2024.105374.

Alvandi A., Ardestani V. E., 2023: Edge detection of potential field anomalies using the Gompertz function as a high-resolution edge enhancement filter. Bull. Geophys. Oceanogr., **64**, 3, 279–300, doi: 10.4430/bgo00420.

Alvandi A., Su K., Ai H., Ardestani V. E., Lyu C., 2023: Enhancement of potential field source boundaries using the hyperbolic domain (Gudermannian function). Minerals, **13**, 10, 1312, doi: 10.3390/min13101312.

Alvandi A., Ardestani V.E., Motavalli-Anbaran S.-H., 2024: Novel detectors based on the Elliott Function for mapping potent ial field data: Application to aeromagnetic data from Indiana, United States. Ann. Geophys., **67**, 6, GP656, doi: 10.4401/ag-9146.

Alvandi A., Ardestani V. E., Motavalli-Anbaran S.-H., 2025: Enhancement of the total horizontal gradient of potential field data using the Modified Gudermannian Function (MGTHG): application to aeromagnetic data from Georgia, USA. Bull. Geophys. Oceanogr., **66**, 1, 73–94, doi: 10.4430/bgo00479.

Bonvalot S., Briais A., Kuhn M., Peyrefitte A., Vales N., Biancale R., Gabalda G., Moreaux G., Reinquin F., Sarrailh M., 2012: Global grids: World Gravity Map (WGM2012). Bureau Gravimetrique International, doi: 10.18168/bgi.23.

Castro F. R., Oliveira S. P., de Souza J., Ferreira F. J., 2020: Constraining Euler deconvolution solutions through combined tilt derivative filters. Pure Appl. Geophys., **177**, 10, 4883–4895, doi: 10.1007/s00024-020-02533-w.

Cooper G. R. J., Cowan D. R., 2006: Enhancing potential field data using filters based on the local phase. Comput. Geosci., **32**, 10, 1585–1591, doi: 10.1016/j.cageo.2006.02.016.

Cordell L., Grauch V. J. S., 1985: Mapping basement magnetization zones from aeromagnetic data in the San Juan Basin, New Mexico. In: Hinze W. J.: The utility of regional gravity and magnetic anomaly maps, pp. 181–197, Society of Exploration Geophysicists, doi: 10.1190/1.0931830346.ch16.

Deniz Toktay H., Prasad K. N. D., Alvandi A., 2024: Edge enhancement of potential field data using the enhanced gradient (EG) filter. Bull. Miner. Res. Explor., **174**, 55–66, doi: 10.19111/bulletinofmre.1386653.

Ekinci Y. L., Balkaya Ç., Göktürkler G., Ai H., 2023: 3-D gravity inversion for the basement relief reconstruction through modified success-history-based adaptive differential evolution. Geophys. J. Int., **235**, 1, 377–400, doi: 10.1093/gji/ggad222.

Ekwok S. E., Eldosouky A. M., Ben U. C., Alzahrani H., Abdelrahman K., Achadu O.-I. M., Pham L. T., Akpan A. E., Gómez-Ortiz D., 2022a: Application of high-precision filters on airborne magnetic data: A case study of the Ogoja Region, Southeast Nigeria. Minerals, **12**, 10, 1227, doi: 10.3390/min12101227.

Ekwok S. E., Eldosouky A. M., Achadu O.-I. M., Akpan A. E., Pham L. T., Abdelrahman K., Gómez-Ortiz D., Ben U. C., Fnais M. S., 2022b: Application of the enhanced horizontal gradient amplitude (EHGA) filter in mapping of geological structures involving magnetic data in southeast Nigeria. J. King Saud Univ. Sci, **34**, 8, 102288, doi: 10.1016/j.jksus.2022.102288.

Eldosouky A. M., Pham L. T., Henaish A., 2022: High precision structural mapping using edge filters of potential field and remote sensing data: A case study from Wadi Umm Ghalqa area, South Eastern Desert, Egypt. Egypt. J. Remote Sens. Space Sci., **25**, 2, 501–513, doi: 10.1016/j.ejrs.2022.03.001.

Eldosouky A. M., Eleraki M., Mansour A., Saada S. A., Zamzam S., 2024a: Geological controls of mineralization occurrences in the Egyptian Eastern Desert using advanced integration of remote sensing and magnetic data. Sci. Rep., **14**, 16700, doi: 10.1038/s41598-024-66924-y.

Eldosouky A. M., Othman A., Saada S. A., Zamzam S., 2024b: A new vector for mapping gold mineralization potential and proposed pathways in highly weathered basement rocks using multispectral, radar, and magnetic data in random forest algorithm. Nat. Resour. Res., **33**, 1, 23–50, doi: 10.1007/s11053-023-10292-3.

Elhussein M., Diab Z. E., 2023: Gravity data imaging using local wavenumber-based algorithm: Sustainable development cases studies. Nat. Resour. Res., **32**, 1, 171–193, doi: 10.1007/s11053-022-10137-5.

Elhussein M., Diab Z. E., 2025: Highly efficient gravity data inversion using the TG-GPSO algorithm: Applications in volcanic activity and geothermal exploration studies. Arab. J. Sci. Eng., **2025**, 1–27, doi: 10.1007/s13369-024-09841-6.

Farhi W., Eldosouky A. M., Mickus K., Belkhiria W., Pham L. T., Amar B., 2025: Implementation of gravity and magnetic methods for understanding the structural configuration of the Neogene Lower Chelif Basin (LCB), Northern Algerian Margin. Ital. J. Geosci., 144, 1, 5–21, doi: 10.3301/IJG.2024.24.

Fattahi M., Walker R. T., Talebian M., Sloan R. A., Rasheedi A., 2011: The structure and late Quaternary slip rate of the Rafsanjan strike-slip fault, SE Iran. Geosphere, **7**, 5, 1159–1174, doi: 10.1130/GES00651.1.

Ferreira F. J. F., de Souza J., de Barros e Silva Bongiolo A., de Castro L. G., 2013: Enhancement of the total horizontal gradient of magnetic anomalies using the tilt angle. Geophysics, **78**, 3, J33–J41, doi: 10.1190/geo2011-0441.1.

Florio G., Fedi M., Pasteka R., 2006: On the application of Euler deconvolution to the analytic signal. Geophysics, **71**, 6, L87–L93, doi: 10.1190/1.2360204.

Ghiasi S. M., Hosseini S. H., Afshar A., Abedi M., 2023: A novel magnetic interpretational perspective on Charmaleh iron deposit through improved edge detection techniques and 3D inversion approaches. Nat. Resour. Res., **32**, 1, 147–170, doi: 10.1007/s11053-022-10135-7.

Hamimi Z., Eldosouky A. M., Hagag W., Kamh S. Z., 2023: Large-scale geological structures of the Egyptian Nubian Shield. Sci. Rep., **13**, 1923, doi: 10.1038/s41598-023-29008-x.

Hosseini S. H., Afshar A., Ostadmahdi Aragh N., 2024: The innovative application of gravity data inversion and geophysical edge-detection for celestine exploration: A case study at the Siraf Mine, Semnan Province, Iran. Int. J. Min. Geo-Eng., **58**, 4, 383–390, doi: 10.22059/ijmge.2024.380299.595185.

Hosseininia M., Hassanzadeh R., 2023: Groundwater quality assessment for domestic and agricultural purposes using GIS, hydrochemical facies and water quality indices: case study of Rafsanjan plain, Kerman province, Iran. Appl. Water Sci., **13**, 3, 84, doi: 10.1007/s13201-023-01891-9.

Ma G., Huang D., Liu C., 2016: Step-edge detection filters for the interpretation of potential field data. Pure Appl. Geophys., **173**, 3, 795–803, doi: 10.1007/s00024-015-1053-6.

Miller H. G., Singh V., 1994: Potential field tilt—a new concept for location of potential field sources. J. Appl. Geophys., **32**, 2-3, 213–217, doi: 10.1016/0926-9851(94)90022-1.

Nasuti Y., Nasuti A., Moghadas D., 2019: STDR: A novel approach for enhancing and edge detection of potential field data. Pure Appl. Geophys., **176**, 2, 827–841, doi: 10.1007/s00024-018-2016-5.

Oliveira S. P., Pham L. T., 2022: A stable finite difference method based on upward continuation to evaluate vertical derivatives of potential field data. Pure Appl. Geophys., **179**, 12, 4555–4566, doi: 10.1007/s00024-022-03164-z.

Oruç B., 2011: Edge detection and depth estimation using a tilt angle map from gravity gradient data of the Kozaklı-Central Anatolia Region. Turkey. Pure Appl. Geophys., **168**, 10, 1769–1780, doi: 10.1007/s00024-010-0211-0.

Pham L. T., Oksum E., Kafadar O., Trinh P. T., Nguyen D. V., Vo Q. T., Le S. T., 2022: Determination of subsurface lineaments in the Hoang Sa islands using enhanced methods of gravity total horizontal gradient. Vietnam J. Earth Sci., **44**, 3, 395–409, doi: 10.15625/2615-9783/17013.

Pham L. T., Prasad K. N. D., 2023: Analysis of gravity data for extracting structural features of the northern region of the Central Indian Ridge. Vietnam J. Earth Sci., **45**, 2, 147–163, doi: 10.15625/2615-9783/18206.

Rao D. B., Prakash M. J., Babu N. R., 1990: 3D and 2½D modelling of gravity anomalies with variable density contrast. Geophys. Prospect., **38**, 4, 411–422, doi: 10.1111/j.1365-2478.1990.tb01854.x.

Reid A. B., Allsop J. M., Granser H., Millett A. T., Somerton I. W., 1990: Magnetic interpretation in three dimensions using Euler deconvolution. Geophysics, **55**, 1, 80–91, doi: 10.1190/1.1442774.

Richards J. P., Sholeh A., 2016: The Tethyan tectonic history and Cu-Au metallogeny of Iran (Chapter 7). In: Richards J. P. (Ed.): Tectonics and Metallogeny of the Tethyan Orogenic Belt, Society of Economic Geologists, pp. 193–212, doi: 10.5382/SP.19.07.

Saada S. A., Eldosouky A. M., Abdelrahman K., Al-Otaibi N., Ibrahim E., Ibrahim A., 2021: New insights into the contribution of gravity data for mapping the lithospheric architecture. J. King Saud Univ. Sci, **33**, 3, 101400, doi: 10.1016/j.jksus.2021.101400.

Saada S. A., Eleraki M., Mansour A., Eldosouky A. M., 2025: Insights on the structural framework of the Egyptian Eastern Desert derived from edge detectors of gravity data. Interpretation, **13**, 1, T71–T85, doi: 10.1190/int-2024-0023.1.

Salem A., Williams S., Fairhead J. D., Ravat D., Smith R., 2007: Tilt-depth method: A simple depth estimation method using first-order magnetic derivatives. Lead. edge, **26**, 12, 1502–1505, doi: 10.1190/1.2821934.

Thompson D. T., 1982: EULDPH: A new technique for making computer-assisted depth estimates from magnetic data. Geophysics, **47**, 1, 31–37, doi: 10.1190/1.1441278.

Tran K. V., Nguyen T. N., 2020: A novel method for computing the vertical gradients of the potential field: application to downward continuation. Geophys. J. Int., **220**, 2, 1316–1329, doi: 10.1093/gji/ggz524.